Supplementary Materials

Evolution of electronic structure in pristine and Rb-reconstructed surfaces of kagome metal RbV_3Sb_5

Jiawei Yu[†, ‡, ▽], Zian Xu[§, ▽], Kebin Xiao[†, ‡], Yonghao Yuan[†, ‡], Qiangwei Yin[¶], Zhiqiang Hu[†, ‡], Chunsheng Gong[¶], Yunkai Guo[†, ‡], Zhijun Tu[¶], Peizhe Tang[§, #], Hechang Lei[¶, *], Qi-Kun Xue[†, ‡, ⊥, ‖, *] and Wei Li[†, ‡, *]

[†]*State Key Laboratory of Low-Dimensional Quantum Physics, Department of Physics, Tsinghua University, Beijing 100084, China*

[‡]*Frontier Science Center for Quantum Information, Beijing 100084, China*

[§]*School of Materials Science and Engineering, Beihang University, Beijing 100191, China*

[¶]*Department of Physics and Beijing Key Laboratory of Opto-electronic Functional Materials & Micro-nano Devices, Renmin University of China, Beijing 100872, China*

[#]*Max Planck Institute for the Structure and Dynamics of Matter, Center for Free-Electron Laser Science, 22761 Hamburg, Germany*

[⊥]*Beijing Academy of Quantum Information Sciences, Beijing 100193, China*

[‖]*Southern University of Science and Technology, Shenzhen 518055, China*

[▽]These authors contributed equally to this work.

[*]Wei Li Email: weili83@tsinghua.edu.cn

[*]Hechang Lei Email: hlei@ruc.edu.cn

[*]Qi-Kun Xue Email: qkxue@mail.tsinghua.edu.cn

1. Annealing experiment

We transferred the sample out of STM head (4 K), and annealed it at room temperature; Then the sample was transferred back to STM and measured again. This is an annealing cycle (Figure S1a). Annealing process (with multiple cycles) is shown in Figure S1b. The pristine surface is Rb-1×1 with few Rb-vacancy (Figure S1c). With increased annealing time, a large amount of Rb-vacancies appears firstly (Figure S1d), then short-range of Rb-√3×1 surface starts to form with the continuous loss of Rb (Figure S1e, f), and long-range Rb-√3×√3 surface is obtained finally (Figure S1g). The temperature-dependent Rb reconstructions may give rise to various electronic structures.

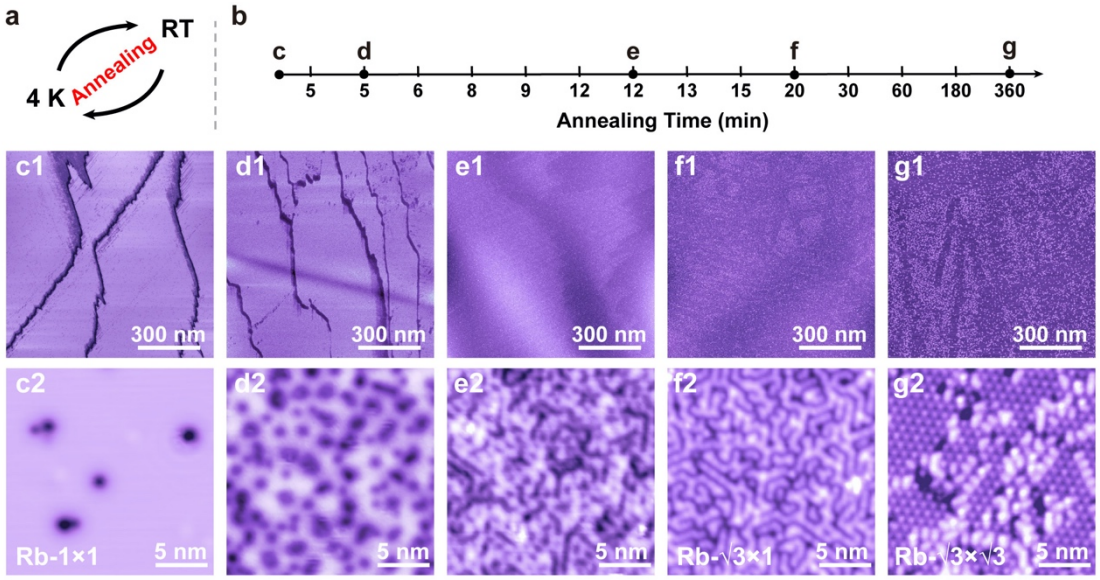

Figure S1. Annealing experiment of RbV_3Sb_5. (a) Schematic of an annealing cycle. (b) Annealing process of the sample. The number on time axis represents the annealing time for a single cycle. Representative STM topographies of the annealing experiment are shown in (d-g). (c1, c2) STM topographies of the pristine Rb surface. Set point: (c1) 1 um × 1 um, bias voltage V_s = -300 mV, tunnelling current I_t = 20 pA; (c2) 20 nm × 20 nm, V_s = -200 mV, I_t = 0.1 nA. (d1-g1) Topographies of Rb surface (1 um × 1 um, V_s = -300 mV, I_t = 20 pA) under the annealing cycle **d-g** labeled in (b). (d2-g2) Corresponding zoom-in topographic images of (d1-g1) (V_s = -300 mV, I_t = 20 pA), in which the desorption of Rb can be clearly observed: More Rb-vacancies appear in (d2); Short-range Rb-√3×1 reconstruction forms in (e2) and (f2); And finally Rb-√3×√3 reconstruction shows up in (g2).

2. Computational Methods and the electronic states for the bulk structure and Rb-1×1 thin film.

The density functional theory (DFT) calculations were simulated by using the Vienna *Ab Initio* Simulation package (VASP)[1]. The projector-augmented-wave method[2, 3] was employed, and we used the generalized-gradient approximation (GGA) of Perdew-Burke-Ernzerhof type exchange-correlation functional[4] with the energy cutoff of 350 eV. The convergence for the electronic self-consistent calculations was set as 10^{-6} eV. Four lattice structures for RbV_3Sb_5 were considered in this work, including bulk structure, thin films of Rb-1×1, Rb-√3×1, and Rb-√3×√3 with the thickness of three unit-cells. For the bulk structure, we fully relaxed its structure until the forces were less than 0.01 eV/Å, and we obtained the lattice constants for *a* (*b*) as 5.426 Å and *c* as 9.081 Å, which were consistent with our experimental observations. For thin-film structures, a vacuum layer with 20 Å was added along the z direction. During the relaxation, we fixed inner atoms with the thickness of one unit-cell and let other atoms fully relax (including top and bottom surfaces). The DFT-D3 method is used for the correction of van der Waals interactions[5]. The K-point meshes were set to 10 × 10 × 6, 10 × 10 × 1, 10 × 6 × 1, and 6 × 6 × 1 for the bulk structure, Rb-1×1, Rb-√3×1, and Rb-√3×√3 thin films, respectively. The band-unfolding results[6] of Rb-√3×1, and Rb-√3×√3 thin film structures are calculated from the PyVaspwfc package[7].

As shown in Figure S2, we plot the orbital-projected band structures for bulk RbV_3Sb_5 and Rb-1×1 thin film. Consistent with previous calculations[8], we find that, for the bulk state, electron-like states around the Γ point are mainly contributed by the p_z orbitals of Sb atoms and states around the M point near the Fermi level are mainly from the *d* orbitals of V atoms. Due to the quantum confinement effect in thin films, states around the Γ point split into quantum well states (pointed by the blue arrow). Meanwhile, around the M point, the bands mainly contributed by the *d* orbital of V atoms also split into a bunch of quantum well states near the Fermi surface, which are marked by the purple rectangle. Interestingly, the center of quantum well states at the M point is close to the energy of the *d* orbitals of V atoms in the bulk. Once we clarify the physical origin for these states around the Fermi level, we could monitor their change corresponding to the variation of Rb coverage on the topmost surface.

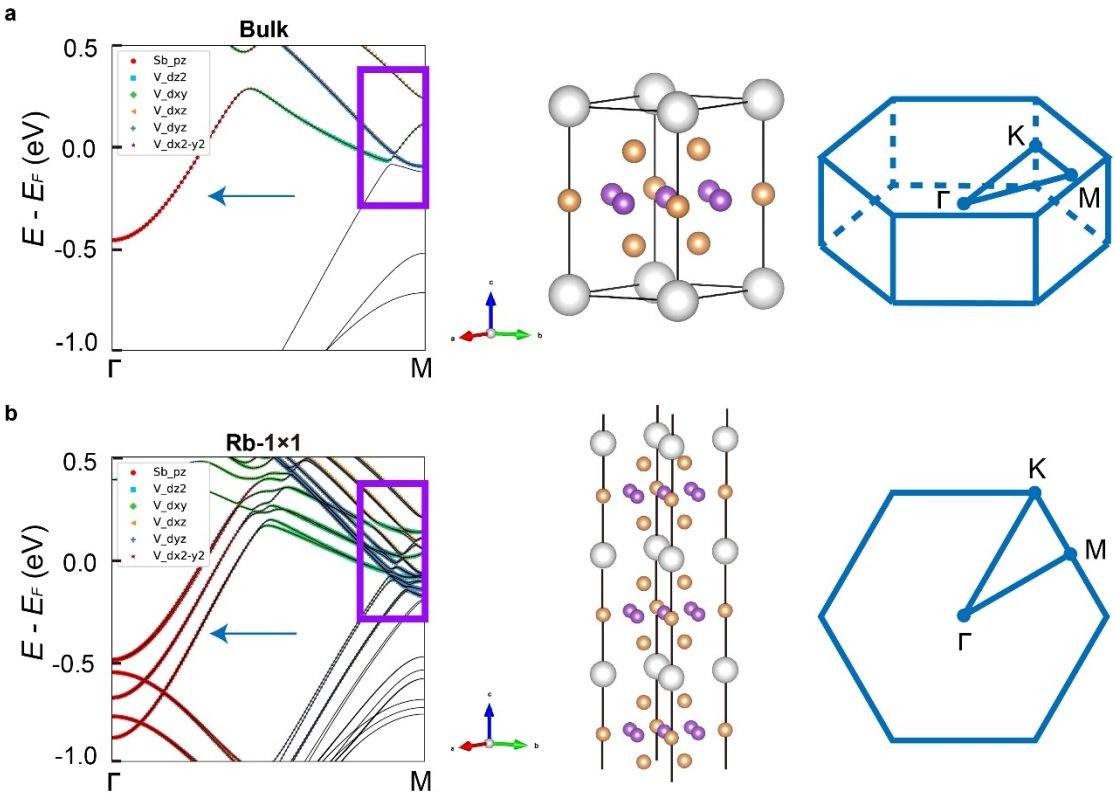

Figure S2. The band structures of bulk RbV_3Sb_5 and Rb-1×1 thin film. (a) Left: the orbital-projected band structures for bulk RbV_3Sb_5 along Γ-M direction. The blue arrow indicates the state at the Γ point contributed by Sb atoms, and the purple rectangle marks the states at the M point contributed by V atoms near the Fermi surface. Middle: the side view of the bulk RbV_3Sb_5 structure. Right: the first BZ of the bulk structure. (b) Left: the orbital-projected band structure of Rb-1×1 along Γ-M direction. Middle: the side view of Rb-1×1 thin film. Right: the first BZ of Rb-1×1 thin film. The calculated Fermi levels are set as zero.

3. The electronic states for Rb-1×1, Rb-√3×1, Rb-√3×√3 thin films

We calculate the orbital-projected band structures for Rb-1×1, Rb-√3×1, Rb-√3×√3 thin films, as shown in Figure S3, which are projected to Sb bottoms surfaces and Rb topmost surfaces. Due to the surface reconstructions, the BZs of Rb-√3×1, Rb-√3×√3 thin films are smaller than that for Rb-1×1 thin film (see Figure. S3d). For these states contributed by top and bottom surfaces, we choose one unit cell as the thickness cutoff. For example, we treat these states contributed by the top surface with the thickness of one unit cell as the surface state from the topmost Rb surface. From Figure S3, we conclude the values of ΔE_{ud} for each thin film model, as shown in Figure 6c in the main text.

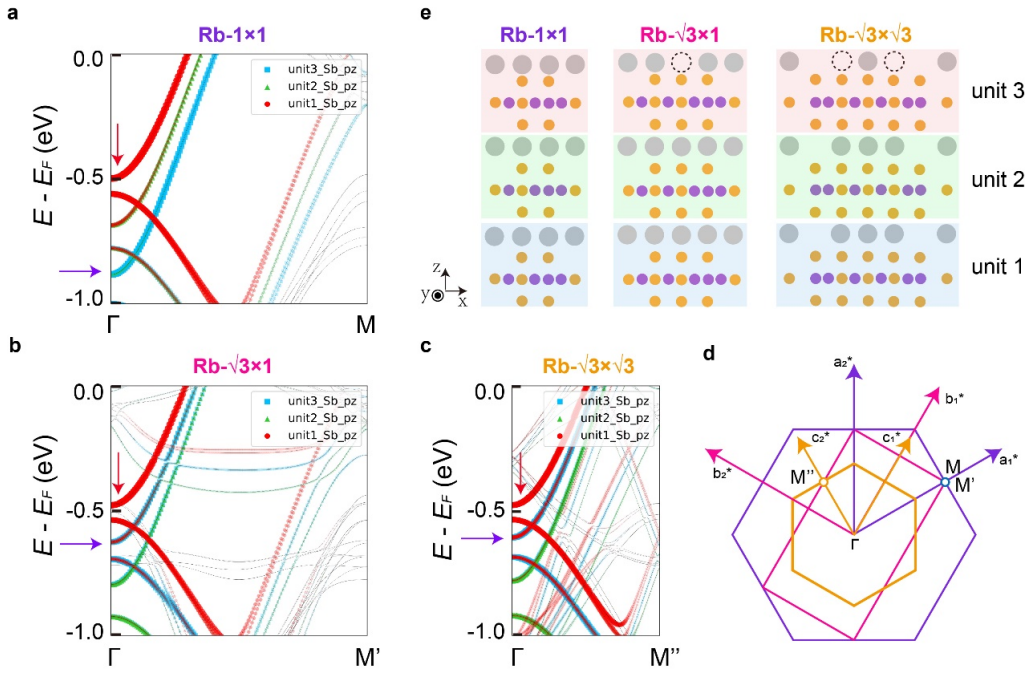

Figure S3. The orbital-projected band structures of three thin-film models. (a-c) Orbital projected band structures for three thin-film models, respectively. Red arrows indicate states at the Γ point from the Sb bottom surfaces, and purple arrows indicate states at the Γ point from the topmost Rb surfaces in each thin-film structure. (d) The first BZ for Rb-1×1 (purple), Rb-√3×1 (pink), and Rb-√3×√3 (yellow) thin films, respectively, specified by various colors. (e) the side views of three thin-film structures. We plot the top, middle, bottom unit cell with different backgrounds, whose colors are corresponding to the color dots shown in band structures.

4. Effective masses of electron-like states around the Γ point

By using the DFT calculations, we obtain the effective masses for electron-like states around the Fermi level with different reconstructed Rb surfaces, whose values are also calculated from the QPI results as shown in the main text and Figure. S4b. In Figure S4a, we show the band structures along the Γ-M direction in the original BZ of Rb-1×1 thin film, which are contributed by p_z orbitals of Rb atoms on each surface with different Rb surface reconstructions. For each thin film model with reconstruction on the Rb surface, we could obtain the energy dispersions on the bared Sb surface (dashed lines with different colors shown in Figure. S4a) and the Rb surface (solid lines with different colors shown in Figure. S4a). We find that although electronic states contributed by bared Sb surfaces in each slab model do not overlap perfectly, they stay in the same energy range and share the similar energy dispersions. Such fact indicates that the reconstruction on Rb surfaces in thin films will influence little to electronic states on bared Sb surfaces. In Figure. S4c, we plot the calculated effective masses for states on different surfaces and compare them with results obtained from QPI data. The tendency of the effective masses with the decreasing of Rb atoms' coverage is consistent with experimental results very well. Especially for the Rb-√3×1 model, the simulated effective mass is smaller than that from Rb-√3×√3 model. Such results match with the experimental observation. We conclude that the hole doping is not the only physical origin for the change of the Fermi surface, and the atomic reconstructions on the surface will also influence the electronic properties of these states on the Rb surfaces.

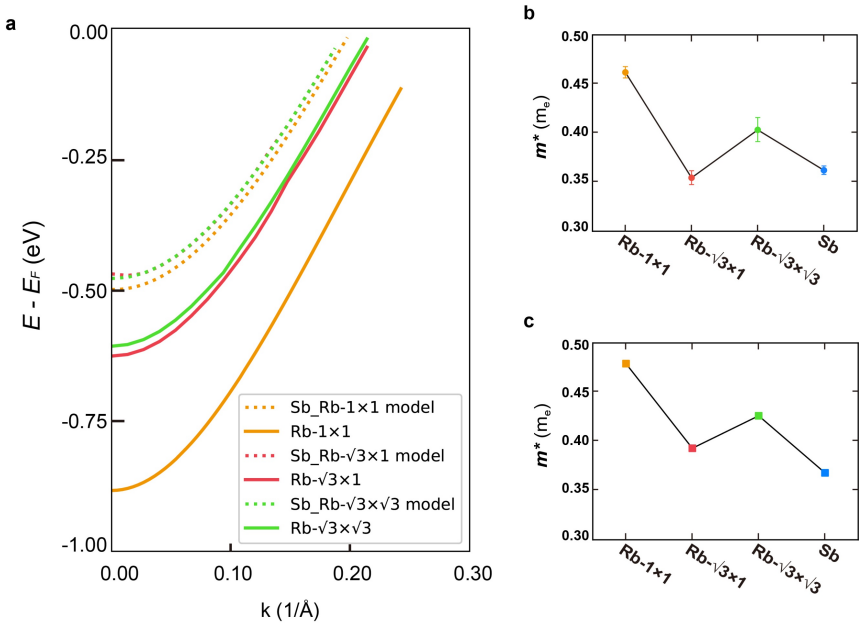

Figure S4. The calculated band structures and corresponding effective masses were obtained from three thin-film models. (a) Calculated band structures without and with band-unfolding for Rb-1×1, Rb-√3×1, and Rb-√3×√3 thin films along the Γ-M direction in the original BZ of Rb-1×1 thin film. Effective mass for each surface, including Rb-1×1(orange), Rb-√3×1 (red), Rb-√3×√3 (green) and bared Sb surface (blue), estimated from (b) experimental data and (c) DFT calculated results, respectively.

References

(1) Kresse, G.; Furthmüller, J. Efficient iterative schemes for ab initio total-energy calculations using a plane-wave basis set. *Phys. Rev. B* **1996,** *54*, 11169-11186.

(2) Blöchl, P. E. Projector augmented-wave method. *Phys. Rev. B* **1994,** *50*, 17953-17979.

(3) Kresse, G.; Joubert, D. From ultrasoft pseudopotentials to the projector augmented-wave method. *Phys. Rev. B* **1999,** *59*, 1758-1775.

(4) Perdew, J. P.; Burke, K.; Ernzerhof, M. Generalized Gradient Approximation Made Simple. *Physical Review Letters* **1996,** *77*, 3865-3868.

(5) Grimme, S.; Antony, J.; Ehrlich, S.; Krieg, H. A consistent and accurate ab initio parametrization of density functional dispersion correction (DFT-D) for the 94 elements H-Pu. *The Journal of Chemical Physics* **2010,** *132*, 154104.

(6) Popescu, V.; Zunger, A. Extracting E versus $\vec{k}$ effective band structure from supercell calculations on alloys and impurities. *Phys. Rev. B* **2012,** *85*, 085201.

(7) Zheng, Q. J. Vasp band unfolding https://github.com/QijingZheng/VaspBandUnfolding (accessed Nov.27, 2021).

(8) Liu, Z.; Zhao, N.; Yin, Q.; Gong, C.; Tu, Z.; Li, M.; Song, W.; Liu, Z.; Shen, D.; Huang, Y.; Liu, K.; Lei, H.; Wang, S. Charge-Density-Wave-Induced Bands Renormalization and Energy Gaps in a Kagome Superconductor RbV_3Sb_5. *Phys. Rev. X* **2021,** *11*, 041010.